Optimization of a blueprint for in vitro glycolysis by metabolic real-time analysis

Bujara, Matthias; Schümperli, Michael; Pellaux, René; Heinemann, Matthias; Panke, Sven

Published in:
Nature Chemical Biology

DOI:
10.1038/nchembio.541

nature chemical biology

ARTICLE

PUBLISHED ONLINE: 20 MARCH 2011 | DOI: 10.1038/NCHEMBIO.541

Optimization of a blueprint for *in vitro* glycolysis by metabolic real-time analysis

Matthias Bujara[1], Michael Schümperli[2], René Pellaux[1,2], Matthias Heinemann[2,3] & Sven Panke[1,2]*

Recruiting complex metabolic reaction networks for chemical synthesis has attracted considerable attention but frequently requires optimization of network composition and dynamics to reach sufficient productivity. As a design framework to predict optimal levels for all enzymes in the network is currently not available, state-of-the-art pathway optimization relies on high-throughput phenotype screening. We present here the development and application of a new *in vitro* real-time analysis method for the comprehensive investigation and rational programming of enzyme networks for synthetic tasks. We used this first to rationally and rapidly derive an optimal blueprint for the production of the fine chemical building block dihydroxyacetone phosphate (DHAP) via *Escherichia coli*'s highly evolved glycolysis. Second, the method guided the three-step genetic implementation of the blueprint, yielding a synthetic operon with the predicted 2.5-fold–increased glycolytic flux toward DHAP. The new analytical setup drastically accelerates rational optimization of synthetic multienzyme networks.

Synthetic systems require optimization, no matter whether the design objective is a genetic circuit or a biocatalytic network. Fine tuning of network dynamics turns out to be key for genetic circuit function[1–3] and the direction of fluxes through synthetic or endogenous metabolic pathways[3–5]. Although more and more methods for rational manipulation of system dynamics have become available[5,6] and elaborated computational models for the understanding of system behavior have been developed[7,8], they do not yet allow drawing a detailed blueprint of what to change and how to implement it. Consequently, recent examples of metabolic network fine-tuning have applied evolutionary strategies and high-throughput screening of phenotypes to circumvent the laborious construction and analysis of multiple variants suggested by rational approaches[3,6,9].

Although the construction of different prototypes is facilitated by *de novo* or recursive DNA synthesis[10], the comprehensive experimental testing for follow-up optimization rounds remains laborious[11–13]. For example, the quantitative investigation of metabolic reaction networks is most comprehensively achieved by a combination of chromatography of extracted metabolites and MS analysis[14,15]. Here, laborious sample preparation and subsequent lengthy chromatographic processing of samples (frequently numbering in the hundreds) are time limiting, and the acquisition of dynamic data after perturbations requires an advanced experimental set-up[12,13,16,17].

Complex *in vitro* reaction networks can perform rather advanced synthetic tasks, ranging from multienzyme catalysis to cell-free protein synthesis[18,19]. They can be assembled from multiple purified parts[20,21] or from cell-free extract (CFX)–based systems[19,22]. CFX-based systems benefit from the possibility of recruiting complex systems from a single cultivation. To fully exploit the advantage of using a single cultivation for multienzyme catalysis, the exact optimal network composition has to be preprogrammed genetically into the production host.

In this contribution, we demonstrate how the optimization of cell-free systems can benefit directly from the implementation of an online *in vitro* analysis system[23,24] by first determining a blueprint for the optimization and subsequent genetic implementation as a synthetic operon. Following this procedure allowed us to triple the production of dihydroxyacetone phosphate from glucose by using a synthetic operon comprising four genes.

RESULTS

Measurement setup

We have developed a metabolic real-time analysis tool and integrated it into the workflow for *in vitro* reaction network optimization. In this workflow, bacterial cells are grown and disrupted, and the resulting CFX is used in a continuously stirred enzyme membrane reactor (EMR) for optimization studies, which in turn guide the modifications for the next network generation. In our tool, the outlet stream from the suitably perturbed reaction network in the reactor is diluted and analyzed without further sample preparation in real time by multiple-reaction monitoring in an ESI-MS triple quadrupole mass spectrometer (**Fig. 1**). The system described here operates continuously—that is, substrates are continuously replenished via the inflow into the reactor while substrates, products and intermediates are continuously removed via the outflow. After a reaction in the reactor is initiated, the concentrations of substrates, products and intermediates change over time until a steady state is reached when concentrations are constant. At steady state, the reaction rates for the various reactions are constant and can be directly calculated from steady-state concentrations (**Fig. 1**). It should be mentioned that the *in vitro* setup allows a highly flexible perturbation design, such as the addition of a defined amount of an intermediate for a limited time (pulse additions of intermediates). Addition of enzyme to the reactor leads to a stepwise and long-term increase in enzyme activity (step perturbation of enzymes) because the enzyme is retained inside by the membrane (**Fig. 1**).

To verify the accuracy of the method, we have addressed questions regarding (i) compound identifiability, (ii) quantification accuracy, (iii) reactor dynamics and (iv) ion suppression effects (**Supplementary Methods**). To illustrate the principle, we recorded the dynamic system response of *E. coli*'s *in vitro* glycolysis using a continuous feed of glucose, ATP and NAD^+ as substrates. The investigated reaction system comprised ten enzyme-catalyzed reactions with 18 metabolites, 15 of which were analyzed online by metabolic real-time analysis. CFX from *E. coli* cells grown on yeast extract and glucose was injected as a step perturbation to start the reaction cascade (**Fig. 2**). The dynamics of the various pathway intermediates (**Fig. 2a**) as well as the energy and redox

[1]Department of Biosystems Science and Engineering, ETH Zürich, Basel, Switzerland. [2]Department of Mechanical and Process Engineering, Institute of Process Engineering, ETH Zürich, Zürich, Switzerland. [3]Groningen Biomolecular Sciences and Biotechnology Institute, University of Groningen, Groningen, The Netherlands. *e-mail: sven.panke@bsse.ethz.ch

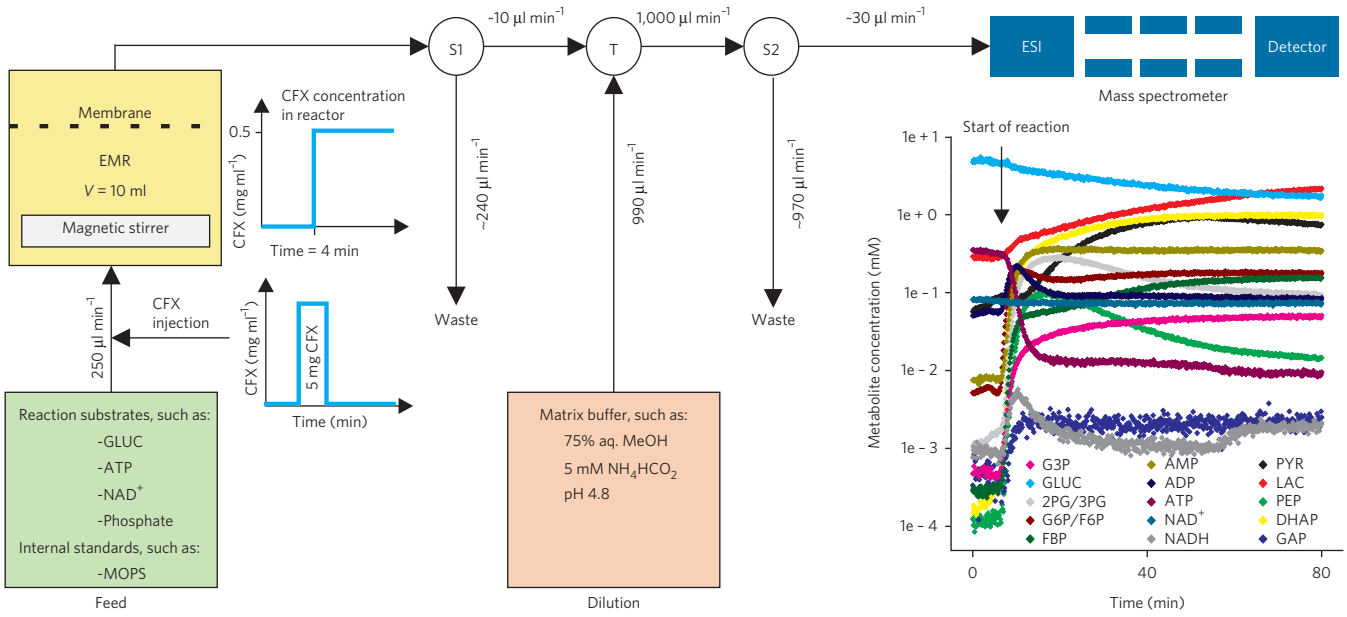

Figure 1 | Setup for MS-based quantitative real-time analysis. The outlet flow of a continuous stirred EMR is continuously analyzed by multiple reaction monitoring in an ESI-triple-quadrupole mass spectrometer after flow reduction (S1), dilution (T) and another flow reduction (S2).

equivalents (**Fig. 2b,c**) can be accurately obtained at a high data density—in this example, at a time resolution of one complete dataset measurement every 8 s. Higher time resolutions can also be applied but only at the expense of increased noise (**Supplementary Methods**). Effectively, the method allows the acquisition of a set of 15 concentrations in less than 10 s, which compares rather favorably with alternative measurement methods for metabolic reaction networks[11–13]. Specifically, it can be used as a highly visual method

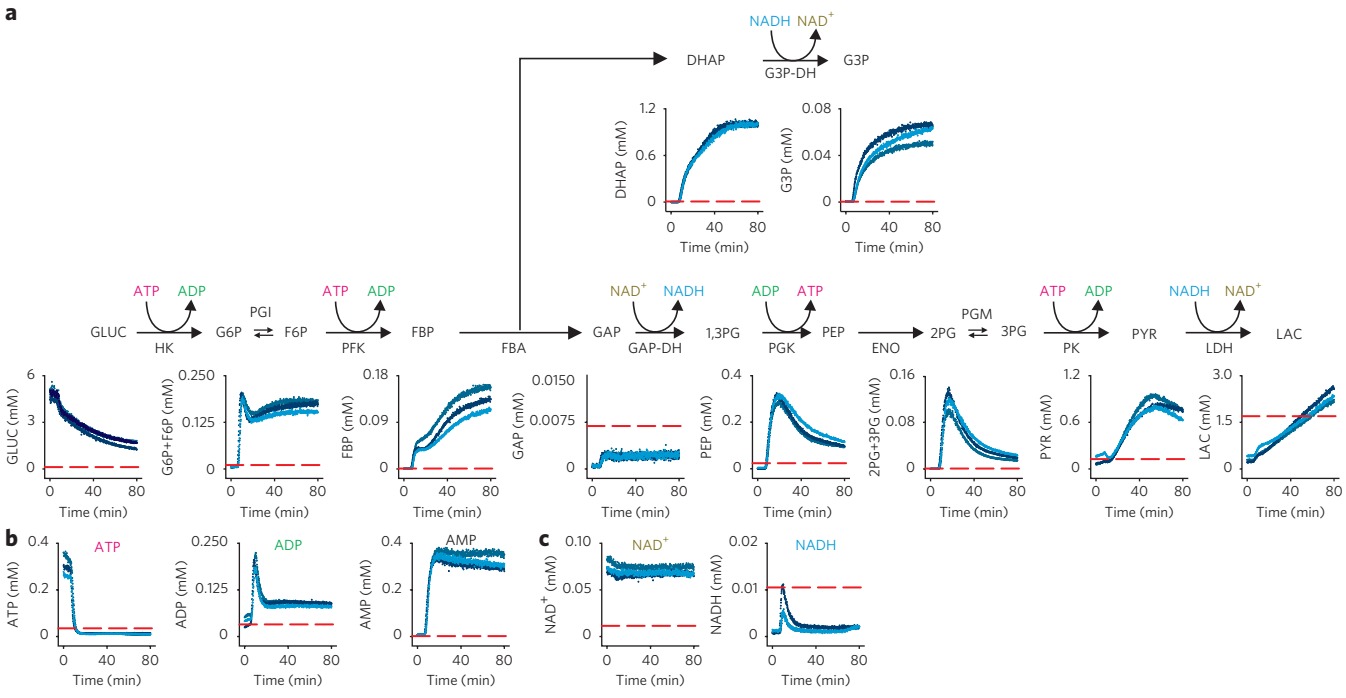

Figure 2 | Quantitative metabolic real-time analysis of *in vitro* multienzyme network dynamics for a glycolytic network engineered for the production of DHAP with integrated cofactor regeneration. (**a**) Detailed dynamics of pathway intermediates of the DHAP production network. (**b**) Cofactor time courses of adenosine phosphate energy carriers. (**c**) Cofactor time courses of NAD^+/NADH redox cofactors. Red dotted lines indicate the limit of quantification (LOQ, signal/noise = 10). Cell-free extract of *E. coli* W3110 Δ*amn tpiA ::Kn* supplemented with commercially available HK, FBA and LDH was used. Metabolite time courses for three consecutive experiments are shown. Phosphoglucose isomerase, PGI; phosphofructokinase, PFK; glyceraldehyde-3-phosphate dehydrogenase, GAP-DH; phosphoglycerate kinase, PGK; phosphoglycerate mutase, PGM; enolase, ENO; pyruvate kinase, PK; glycerol-3-phosphate dehydrogenase, G3P-DH; glucose, GLUC; glucose-6-phosphate, G6P; fructose-6-phosphate, F6P; fructose-1,6-bisphosphate, FBP; dihydroxyacetone phosphate, DHAP; glyceraldehyde-3-phosphate, GAP; 1,3-diphosphoglycerate, 1,3PG; 3-phosphoglycerate, 3PG; 2-phosphoglycerate, 2PG; phosphoenolpyruvate, PEP; pyruvate, PYR; lactate, LAC; hexokinase, HK.

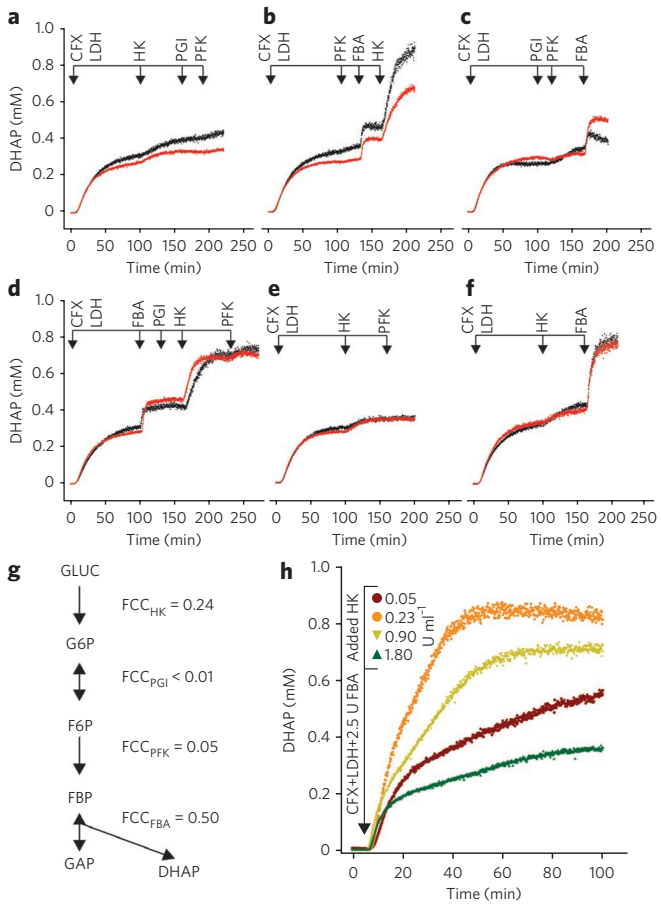

Figure 3 | Identification of rate-limiting steps for DHAP production in the upper part of *E. coli*'s engineered *in vitro* glycolysis (on the basis of CFX of W3110 Δ*amn tpiA:Kn*). (**a**–**f**) All 16 possible combinations of purified enzyme additions were realized in six runs. Reactions were started by CFX injection and subsequent stepwise addition of the corresponding enzyme as indicated. Graphs show DHAP concentration time courses from duplicate experiments. Enzyme sources: HK and PGI, *S. cerevisiae*; PFK, *B. stearothermophilus*; FBA, rabbit muscle. (**g**) Flux control coefficients were calculated for the upper part of glycolysis after the addition of the corresponding single enzyme. It is important to emphasize that the control coefficients reported here describe the flux control of the reference system before the addition of any enzyme, meaning that the control coefficient for a given reaction (for example, HK) after addition of the enzyme is different from the value reported here. (**h**) Modulation of HK activity shows the existence of a local optimal HK concentration in the system with respect to DHAP production. Hexokinase, HK.

to follow the effect of specific network modifications and can accurately assess their impact on overall network performance.

Real-time optimization of *in vitro* glycolysis

We used metabolic real-time analysis to derive a blueprint for a synthetic operon that optimizes the *in vitro* production of the versatile monosaccharide building block DHAP[25] using *E. coli*'s glycolytic network (**Fig. 2a**). As a starting point for system engineering, we used an endogenous network from CFX of a strain carrying a *tpiA-amn* double knockout. The knockout of the triosephosphate isomerase gene (*tpiA*) is necessary because the isomerase would prohibit DHAP accumulation by channeling DHAP to the lower part of glycolysis[22]. The AMP-nucleosidase gene (*amn*) was removed because the reaction is the first step in the conversion of AMP to DHAP and decreases the adenosine phosphate pool (which is the sum of ATP, ADP and AMP)[22]. An *amn* knockout increases the stability of the cofactor ATP by preventing the hydrolysis of AMP[22], which is continuously regenerated in the network[22]. The lactate dehydrogenase (LDH) reaction is necessary to regenerate NADH, which is generated in the lower part of glycolysis, to NAD^+. At this point LDH was added as a purified enzyme, because the *E. coli* LDH is not produced under the aerobic cultivation conditions used for CFX production. Unexpectedly, the addition of hexokinase was not required for *in vitro* system operation, presumably because the applied growth conditions typically do not lead to repression of the endogenous glucokinase[22] gene. In summary, *E. coli* CFX from a *tpiA-amn* knockout strain provides a fully functional glycolytic network that can be used to produce DHAP from glucose with modest ATP supply. An integral part of this system is the regeneration of ATP, which is consumed in the upper part of glycolysis and then regenerated in the lower part of glycolysis by converting glyceraldehyde-3-phosphate (GAP) to lactate (LAC) (**Fig. 2a**).

To obtain a first indication on rate-limiting reactions in the cascade, we calculated flux control coefficients (FCCs) from transient datasets after perturbation with CFX. Notably, FCCs with regard to DHAP production reproducibly indicated an important role for hexokinase and fructose bisphosphate aldolase (FBA), even though FCC calculation from transient metabolite data is known to be sensitive to even small experimental errors[26] (**Supplementary Results**, **Supplementary Table 1**). Next, we investigated the issue of flux control more systematically by a comprehensive series of enzyme concentration perturbations. We used commercially available enzyme preparations that originated from different organisms (**Supplementary Table 2**) with slightly different kinetic properties to selectively increase the reaction rate of a single reaction. All possible combinations of enzyme additions from the upper part of glycolysis and all meaningful combinations of enzymes additions from the lower part were realized. For this, the reaction cascade was started by CFX injection, the DHAP concentration was allowed to reach steady state, and a first purified enzyme was added in excess. When the steady state had been reached again, another enzyme could be added to investigate the effect of this particular combination, and so on. By following the system behavior online, several step functions with different enzymes could be performed consecutively using the same CFX in the reactor. Metabolic real-time analysis enabled a full factorial screening in the upper part of glycolysis from glucose to DHAP, realizing all 16 possible combinations of the four enzymes involved in only six runs (**Supplementary Methods**) with a total reaction and analysis time of only 18 h, generating more than 8,000 comprehensive sets of intermediate concentrations in this time.

As a single addition, only hexokinase and FBA were capable of increasing DHAP production slightly, validating the distribution of flux control between the two enzymes. The addition of phosphoglucose isomerase (PGI) and phosphofructokinase (PFK) did not affect DHAP production (**Fig. 3a**–**f**). The addition of both hexokinase and FBA increased steady-state concentrations of DHAP by a factor of 2.5, pointing toward a concerted bottleneck in the hexokinase and FBA reactions. Averaged FCCs calculated from single-enzyme addition experiments predicted the behavior of an adapted system accurately: the calculated FCCs of approximately 0.24 for hexokinase and 0.5 for FBA (**Fig. 3g**), based on the corresponding time windows during which only hexokinase or FBA had been added (**Fig. 3d,f**), predicted an increase of DHAP production by a factor of 2.4 when supplying both enzymes, which is in good agreement with the experimental result. Notably, the control coefficients refer to the nonoptimized system and change after enzyme addition. As an additional effect, the reproducibility of *in vitro* metabolite time courses of network intermediates such as phosphoenolpyruvate (PEP)—but not of substrates and products such as DHAP—was

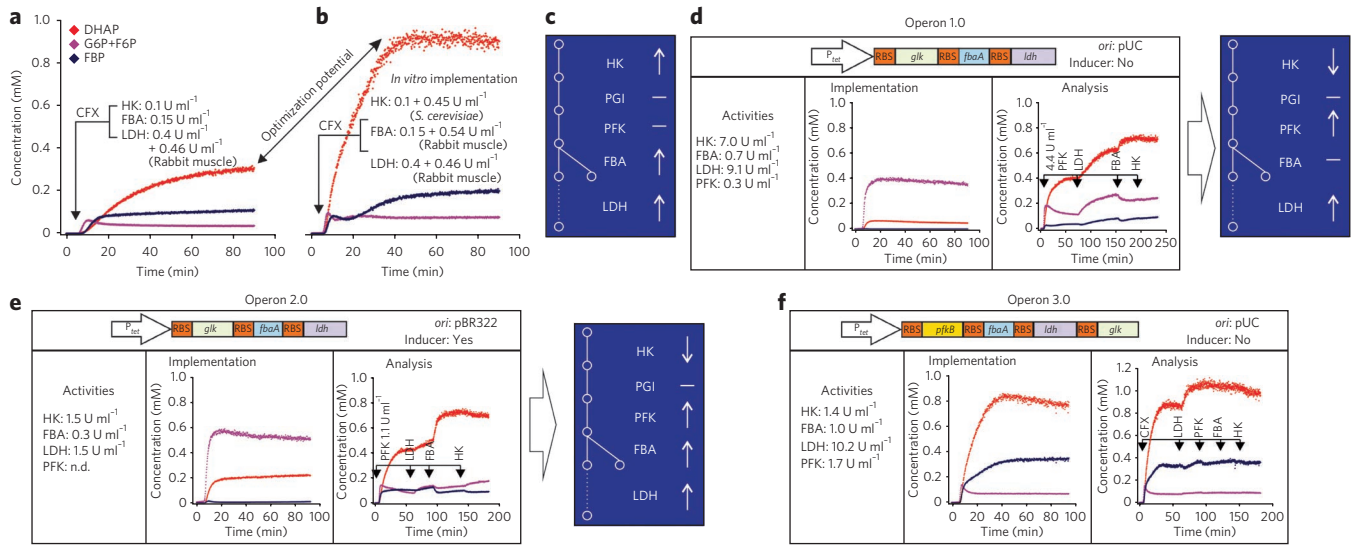

Figure 4 | Operon construction and optimization of *in vivo* expression levels for improved *in vitro* DHAP production in a cell-free system obtained from W3110 Δ*amn tpiA* ::*kn* provided with plasmids as indicated. (**a**) Performance of the endogenous *E. coli* network supplemented *in vitro* with LDH for balanced cofactor recycling. (**b**) The endogenous network supplemented *in vitro* with HK, FBA and LDH. (**c**) A metabolic real-time-analysis–based blueprint for implementing a synthetic operon toward improved DHAP production. (**d**) Performance of an operon expressed from the P_{tet} promoter on a high-copy plasmid containing the *E. coli* genes *glk*, *fbaA* and *ldh*, analysis for rate-limiting reactions and resulting instructions for synthetic operon construction. (**e**) Performance of the operon from **d** expressed from a medium-copy plasmid. (**f**) Incorporation of *pfkB* and changing the gene sequence in the operon produced equally high amounts of DHAP, as suggested by our original blueprint. Experiments were done in duplicate; one representative experiment is shown with only the curves for DHAP (red), G6P (purple) and FBP (blue). Enzyme activities refer to units per ml reactor volume and were determined using *in vitro* assays. Ribosome binding site, RBS.

significantly improved after supplying these two enzymes in excess when compared to a nonoptimized network (**Supplementary Fig. 1**). This was presumably a consequence of the increased robustness of network dynamics after increasing the concentrations of hexokinase and FBA, which can be expected to distribute the flux control over more enzymes.

In a second step, the lower part of glycolysis (from GAP to LAC) was analyzed for rate-limiting steps using the *in vitro*–optimized upper part of glycolysis. The time courses of 2-phosphoglycerate and 3-phosphoglycerate pool (2PG+3PG) and PEP concentrations had always been tightly correlated in previous experiments, suggesting no significant flux control by these reactions (**Supplementary Fig. 2**)[27,28]. Consequently, they were not included in the set of perturbations. A full factorial set of perturbations with the remaining three reactions of the lower part of glycolysis did not show any bottleneck for DHAP production either (**Supplementary Fig. 3**).

Given the apparent importance of hexokinase and FBA for optimal network function and the expected nonlinear nature of the underlying network dynamics[29], it was important to establish whether the observed improvement in DHAP steady-state concentrations could be obtained by a broad range of enzyme concentrations or whether the improvement would depend on a rather narrow window of enzyme concentrations. The hexokinase activity for optimal DHAP production is restricted to a certain window, as indicated by the local maximum in DHAP production as a function of added hexokinase (**Fig. 3h**). A rapid hexokinase reaction consumes most of the ATP provided, leading to high glucose-6-phosphate (G6P) levels (**Supplementary Fig. 4**). Consequently, ATP is limiting for PFK, leading to a reduced pathway flux after G6P[30]. The level of FBA could be reduced by a factor of five, and high DHAP production was still maintained (**Supplementary Fig. 4**). In summary, the blueprint for an operon to improve CFX-based DHAP production by a factor of 2.5 over the endogenous network contained: (i) an increase of hexokinase activity by a factor of approximately four; (ii) an increase of FBA activity by a factor of three (**Fig. 4a–c**); and (iii) the expression of the LDH gene in the synthetic operon, to remove the requirement for adding purified enzyme entirely. The latter is necessary, as mentioned, because LDH is not expressed during aerobic growth of *E. coli* and was up to this point always added as a purified enzyme.

Genetic implementation of the blueprint as an operon

To our knowledge, there is currently no tool available to enable the rational implementation of the blueprint derived above into a synthetic operon. However, metabolic real-time analysis provides an effective tool to quickly identify any deficiency in a synthetic operon and thus delivers clear directions for the next steps toward a sufficiently exact implementation of the blueprint. We started with a prototype operon that expressed the three endogenous *E. coli* genes for the previously identified enzymes (**Fig. 4a–c**) in the order *glk*, *fbaA* and *ldh* from a high-copy plasmid using basal expression from the tetracycline-inducible P_{tet} promoter. Metabolic real-time analysis of the resulting CFX showed ten-fold–reduced DHAP production, a substantially higher production of G6P+F6P and almost no FBP (**Fig. 4d**). This pointed toward the imbalance between the two ATP-consuming enzymes hexokinase and PFK described above (**Fig. 3h**). This hypothesis could be confirmed *in vitro* by supplementing with purified PFK, which increased DHAP levels (**Supplementary Fig. 5**). However, a PFK addition of 4.4 units (U) ml^{-1} as well as additional LDH was necessary to obtain DHAP productivity similar to the earlier *in vitro* optimized system (**Fig. 4d**). Therefore we focused on reducing the hexokinase level first. We next implemented the same operon on a plasmid with a lower copy number. At lower copy number, basal transcription of the synthetic operon from the tetracycline promoter was no longer sufficient, and, consequently, inducer was added (**Supplementary Fig. 6**, **Fig. 4e**). This strategy indeed reduced hexokinase activity relative to the high-copy number situation but still did not allow full compensation of the hexokinase and PFK imbalance (**Fig. 4e**), as DHAP and FBP levels were again low and G6P+F6P levels were again high. LDH activity was

again insufficient, and, additionally, a limitation in the FBA reaction was observed using this operon (**Fig. 4e**).

Because of the narrow hexokinase activity window and the difficulties with exactly meeting the blueprint demands, we decided to incorporate PFK into the operon and also changed the gene sequence. The operon sequence *pfkB*, *fbaA*, *ldh*, *glk* combined with basal expression from the P_{tet} promoter produced equally high concentrations of DHAP, as predicted by our blueprint (**Fig. 4f**, **Supplementary Fig. 6**). This third generation with *pfkB* finally transformed the rational blueprint guidelines into a genetic implementation, enabling high DHAP concentrations without the addition of purified enzymes.

Analyzing this system for potential follow-up optimization rounds revealed that only increasing the LDH concentration could further increase DHAP production. However, the overall LDH activity (in terms of V_{max}) coming from operon expression (~10.2 U ml^{-1}) was already more than 20 times higher than the activity when it was added as a purified enzyme (~0.46 U ml^{-1} of LDH from rabbit muscle) (**Fig. 4f**). A good explanation for this observation is a roughly ten-fold higher K_m for pyruvate of the endogenous *E. coli* LDH used for synthetic operon construction as compared to the rabbit muscle enzyme that had been added as a purified enzyme (**Supplementary Table 2**). Consequently, a different LDH enzyme with a lower K_m value for pyruvate would be the preferred next step for further improvement.

DISCUSSION

Integration of metabolic real-time analysis into the pathway optimization workflow allowed us to draw a detailed operon blueprint for the optimization of *in vitro* DHAP production via *E. coli*'s glycolysis. Although a crucial role for hexokinase and also for PFK could have been anticipated because of their regulatory role in glycolysis[31,32], we could not have predicted the precise combination of pathway modulations that were identified here.

The control of gene expression in (synthetic) operons is rather complex, with multiple regulatory factors controlling absolute enzyme levels and the underlying dynamics of their formation[3,33–36]. Consequently, it is currently impossible to implement a defined set of specifications by designing only a single operon. Therefore, several iterative versions are necessary before the blueprint is implemented. To this end, metabolic real-time analysis makes substantial contributions by reducing the turnaround time between operon generations. A complete dataset, testing a full factorial enzyme perturbation set (**Fig. 3a–f**), can be obtained within two working days, and follow-up analysis of the various operons (for example, **Fig. 4e**) only takes a few hours. This compares favorably to system analysis by LC-MS or other methods and leaves operon construction and modification as the most time-intensive step in the pathway optimization workflow. Recent advances in this area[37] have the potential to reduce the turnaround time for one generation down to a working week.

The major advantage of metabolic real-time analysis is to pinpoint changes in metabolite concentration after perturbation to a certain enzyme in the system context. One prerequisite for this is the availability of purified enzyme preparations for testing their effect on pathway performance. In our case, we used commercially available glycolytic enzymes that originated from other organisms and had different kinetic properties compared to the endogenous *E. coli* enzymes. This reduced the predictive power of the method slightly for the effect of LDH, for example, which remained limiting because of its higher K_m value although it was expressed at a high level. However, in most cases, different enzyme properties as well as availability of enzymes can be easily overcome by using purified endogenous or recombinant enzymes from overproducing strains.

The application demonstrated here used metabolic real-time analysis to optimize relative enzyme levels in a pathway. Under the given set of reaction conditions (such as feed concentrations for ATP and NAD^+), a local optimum for pathway flux was obtained by implementing an operon encoding four genes. Two important questions can be raised concerning the local optimum: (i) whether the local optimum could have been reached with an alternative combination of enzyme levels and (ii) what would be required to turn the local into an absolute maximum. Regarding alternative realizations of the local optimum, our results already indicate that an operon version without PFK but with a tightly adapted expression level of hexokinase would presumably lead to similar results, as our initial blueprint did not indicate a limitation for PFK. Conceptually, our improvements can be described as a systematic elimination of large control coefficients, which inevitably leads to a more distributed pathway control. In other words, further additions of single enzymes can be made, but they will no longer improve pathway fluxes.

The question of the absolute maximum in pathway flux is more difficult to answer. In this contribution, we have focused on adjusting enzyme levels while keeping the reaction conditions constant. Therefore, one obvious way to explore further optimization of pathway flux would be to vary the reaction conditions, such as ATP and NAD^+ concentrations. This would in turn increase the number of required experiments to estimate the potential of a given operon and raises the question of whether metabolic real-time analysis can be adapted to meet such increased experimental demands. The current time resolution between two comprehensive concentration measurements is in the order of 10 s only and can be reduced further. This suggests that metabolic real-time analysis has the potential for multiplexing that would easily support an increased search space.

The integration and insulation of the target network into the cell-free metabolic system is a further important aspect for system performance. For example, the pentose phosphate pathway is known to drain glycolytic intermediates via G6P, F6P and GAP. Although it was known previously that the pentose phosphate pathway is not a major drain for metabolites[22], it might still drain a certain fraction of intermediates and will be a target for further optimization. Improved ATP turnover is another aspect that needs to be addressed in the context of pathway insulation. We have shown previously that deletion of the *amn* gene reduces the conversion of adenosine phosphates to DHAP and other products[22], but clearly much of the provided ATP is still converted to AMP (**Fig. 2b**) without necessarily contributing to system performance. To this end, we are currently implementing methods to largely suppress unrelated ATP hydrolysis.

The method described here offers rapid and comprehensive analysis opportunities in *in vitro* systems with high accuracy. In conclusion, we expect that metabolic real-time analysis will be an important tool in synthetic pathway optimization and that its impact will go beyond even that: the accuracy of this method, its system scope and the freedom to apply an almost unlimited range of user-defined conditions and perturbations (almost any metabolite, matrix component and enzyme) will also help to produce more accurate mechanistic kinetic models for *in silico* prediction of network behavior.

METHODS

General. Chemicals were obtained at the highest purity available and were purchased from Sigma-Aldrich, except for NAD^+ and antibiotics (Gerbu) and yeast extract (BD Bioscience). Purified glycolytic enzymes were from Roche Diagnostics and Sigma-Aldrich.

Mass spectrometry analyses. Mass spectrometry was performed on an Applied Biosystems/MDS Sciex 4000 QTRAP using the Analyst software for data acquisition. The MS was operated in the negative ion and multiple reaction monitoring mode. The settings for ion spray voltage, temperature, curtain gas, collision gas, ion source gas 1 and ion source gas 2 were −4,200 V, 200 °C, 15, 6, 30 and 40 (arbitrary units), respectively. The dwell time was 500 ms, and the settings for declustering potential, collision energy and cell exit potential were optimized separately for each compound using pure standards (**Supplementary Methods**).

Reactor setup. The reactor setup consisted of an injector with a 200-µl injection loop (Rheodyne) and an enzyme membrane reactor with a volume of 10 ml (Jülich Chiral Solutions) stirred at 500 r.p.m. The reactor was fed

by an HPLC pump (HP1050, Agilent Technologies) operated at 250 µl min^{-1}. The flow rate of the reactor outlet was reduced to 10 µl min^{-1} by a pressure drop at a splitting tee (S1, **Fig. 1**) and diluted with matrix buffer from a second HPLC pump operated at 990 µl min^{-1}. After a mixing tee (T, **Fig. 1**) and a frit (0.2 µm), the flow was reduced to 30 µl min^{-1} by a second splitting tee (S2, **Fig. 1**) and injected into the ESI ion source of the mass spectrometer. The parts were connected by fittings and PEEK tubing of the appropriate diameter (Upchurch Scientific, IDEX Health & Science). During membrane reactor assembly, the sequence of spacer plate and membrane was reversed to reduce the dead volume. Details for the reactor setup characterization can be found in **Supplementary Methods**.

Cell-free extract preparation. Cell-free extract was prepared following the procedure reported previously[22]. Briefly, *E. coli* W3110 Δ*amn tpiA*::*kn*[22] was cultivated in a fed-batch bioreactor (5 l) culture using a minimal medium supplemented with glucose (5 g l^{-1}) and yeast extract (5 g l^{-1}) for the batch phase and a feed containing yeast extract, glucose and $MgSO_4$ (100 g l^{-1}, 100 g l^{-1} and 22.2 mM). Cells were harvested by centrifugation in exponential growth phase at an optical density (OD_{600}) of 18–20, resuspended in 10 mM phosphate buffer and disrupted by high pressure homogenization. Insoluble parts were removed by centrifugation; the soluble fraction was frozen in aliquots at −80 °C and used as cell-free extract for analysis.

Analysis. The reactor was fed with a freshly prepared feeding solution (50 mM NH_4HCO_3; 0.5 mM ATP; 0.125 mM NAD^+; 4 mM glucose; 2.5 mM $MgCl_2$; 2 mM Na_2HPO_4; 400 µM MOPS) that contained all important substrates, in particular ATP and NAD^+ for cofactor regenerations and glucose as a starting material for DHAP production. Reactions were carried out at 30 °C throughout the entire experiment. The online experiments were started after the signals for glucose, NAD^+ and ATP had become constant by injecting CFX protein (200 µl of a 25 mg m l^{-1} of total protein solution, optionally supplemented with purified enzymes). Quantification was performed using externally recorded calibration curves (**Supplementary Methods**). Additional enzymes were injected as indicated for each experiment. Note that all enzyme activities mentioned in the text (for both commercially obtained enzymes and activities in cell-free extract) refer to the V_{max} values measured separately but under the same conditions as provided in the experiment (**Supplementary Methods**).

Operon construction. The operons *glk-fbaA-ldh* and *fbaA-ldh-glk* were constructed by sequence-specific recombination in the expression plasmid pASG-IBAwt1 (containing the *tetR* repressor gene) using the StarGate cloning kit and following the supplier's instructions (IBA Biotagnology). The *pfkB-fbaA-ldh-glk* operon was constructed by inserting a PCR-amplified *pfkB* gene in front of *fbaA-ldh-glk*. Replacement of the pASG-IBAwt1-*glk-fbaA-ldh ori* with a PCR fragment containing the pBR322 *ori* allowed changing the plasmid copy number.

Calculation of control coefficients. The general principles of MCA are described in references 38,39. Calculation of FCCs from transient metabolite data was reported previously[40,41] (**Supplementary Methods**). FCCs (C_i) for hexokinase and FBA were calculated from single-enzyme addition experiments according to the large deviation theory using the enzyme activity and flux to DHAP after enzyme addition (E^r and J^r, respectively), the flux change (ΔJ) and the change of enzyme activity (ΔE) as in equation (1).

$$C_i = \frac{\Delta J}{\Delta E_i}\frac{E_i^r}{J^r} \quad (1)$$

The potential relative change in DHAP production (f) was predicted using the control coefficients (C_i^J), the relative increase in the enzyme activity (r_i) and equation (2). In other words, the relative increase of DHAP (f) after increasing the enzyme activity of the i-th reaction by the factor r_i can be calculated when C_i^J for this reaction is known.

$$\frac{(f-1)}{f} = \sum_{i=1}^{n}\left[C_i^J\left(\frac{(r_i-1)}{r_i}\right)\right] \quad (2)$$

Received 13 September 2010; accepted 27 January 2011; published online 20 March 2011

References

1. Anderson, J.C., Clarke, E.J., Arkin, A.P. & Voigt, C.A. Environmentally controlled invasion of cancer cells by engineered bacteria. *J. Mol. Biol.* **355**, 619–627 (2006).
2. Yokobayashi, Y., Weiss, R. & Arnold, F.H. Directed evolution of a genetic circuit. *Proc. Natl. Acad. Sci. USA* **99**, 16587–16591 (2002).
3. Pfleger, B.F., Pitera, D.J., Smolke, C.D. & Keasling, J.D. Combinatorial engineering of intergenic regions in operons tunes expression of multiple genes. *Nat. Biotechnol.* **24**, 1027–1032 (2006).
4. Anthony, J.R. *et al.* Optimization of the mevalonate-based isoprenoid biosynthetic pathway in *Escherichia coli* for production of the anti-malarial drug precursor amorpha-4,11-diene. *Metab. Eng.* **11**, 13–19 (2009).
5. Salis, H.M., Mirsky, E.A. & Voigt, C.A. Automated design of synthetic ribosome binding sites to control protein expression. *Nat. Biotechnol.* **27**, 946–950 (2009).
6. Alper, H., Fischer, C., Nevoigt, E. & Stephanopoulos, G. Tuning genetic control through promoter engineering. *Proc. Natl. Acad. Sci. USA* **102**, 12678–12683 (2005).
7. Hadlich, F., Noack, S. & Wiechert, W. Translating biochemical network models between different kinetic formats. *Metab. Eng.* **11**, 87–100 (2009).
8. Kotte, O., Zaugg, J.B. & Heinemann, M. Bacterial adaptation through distributed sensing of metabolic fluxes. *Mol. Syst. Biol.* **6**, 355 (2010).
9. Wang, H.H. *et al.* Programming cells by multiplex genome engineering and accelerated evolution. *Nature* **460**, 894–898 (2009).
10. Linshiz, G. *et al.* Recursive construction of perfect DNA molecules from imperfect oligonucleotides. *Mol. Syst. Biol.* **4**, 191 (2008).
11. Bennett, M.R. & Hasty, J. Microfluidic devices for measuring gene network dynamics in single cells. *Nat. Rev. Genet.* **10**, 628–638 (2009).
12. El Massaoudi, M., Spelthahn, J., Drysch, A., de Graaf, A. & Takors, R. Production process monitoring by serial mapping of microbial carbon flux distributions using a novel sensor reactor approach: I–Sensor reactor system. *Metab. Eng.* **5**, 86–95 (2003).
13. Buziol, S. *et al.* New bioreactor-coupled rapid stopped-flow sampling technique for measurements of metabolite dynamics on a subsecond time scale. *Biotechnol. Bioeng.* **80**, 632–636 (2002).
14. Büscher, J.M., Czernik, D., Ewald, J.C., Sauer, U. & Zamboni, N. Cross-platform comparison of methods for quantitative metabolomics of primary metabolism. *Anal. Chem.* **81**, 2135–2143 (2009).
15. Bennett, B.D. *et al.* Absolute metabolite concentrations and implied enzyme active site occupancy in *Escherichia coli*. *Nat. Chem. Biol.* **5**, 593–599 (2009).
16. van den Brink, J. *et al.* Dynamics of glycolytic regulation during adaptation of *Saccharomyces cerevisiae* to fermentative metabolism. *Appl. Environ. Microbiol.* **74**, 5710–5723 (2008).
17. van Eunen, K. *et al.* Measuring enzyme activities under standardized *in vivo*-like conditions for systems biology. *FEBS J.* **277**, 749–760 (2010).
18. Woodward, J., Orr, M., Cordray, K. & Greenbaum, E. Biotechnology: Enzymatic production of biohydrogen. *Nature* **405**, 1014–1015 (2000).
19. Jewett, M.C., Calhoun, K.A., Voloshin, A., Wuu, J.J. & Swartz, J.R. An integrated cell-free metabolic platform for protein production and synthetic biology. *Mol. Syst. Biol.* **4**, 220 (2008).
20. Shimizu, Y. *et al.* Cell-free translation reconstituted with purified components. *Nat. Biotechnol.* **19**, 751–755 (2001).
21. Zhang, Y.H.P., Evans, B.R., Mielenz, J.R., Hopkins, R.C. & Adams, M.W.W. High-yield hydrogen production from starch and water by a synthetic enzymatic pathway. *PLoS ONE* **2**, e456 (2007).
22. Bujara, M., Schümperli, M., Billerbeck, S., Heinemann, M. & Panke, S. Exploiting cell-free systems: Implementation and debugging of a system of biotransformations. *Biotechnol. Bioeng.* **106**, 376–389 (2010).
23. Chen, H. & Zenobi, R. Neutral desorption sampling of biological surfaces for rapid chemical characterization by extractive electrospray ionization mass spectrometry. *Nat. Protoc.* **3**, 1467–1475 (2008).
24. Zhu, L. *et al.* Real-time, on-line monitoring of organic chemical reactions using extractive electrospray ionization tandem mass spectrometry. *Rapid Commun. Mass Spectrom.* **22**, 2993–2998 (2008).
25. Schümperli, M., Pellaux, R. & Panke, S. Chemical and enzymatic routes to dihydroxyacetone phosphate. *Appl. Microbiol. Biotechnol.* **75**, 33–45 (2007).
26. Ehlde, M. & Zacchi, G. Influence of experimental errors on the determination of flux control coefficients from transient metabolite concentrations. *Biochem. J.* **313**, 721–727 (1996).
27. Kummel, A., Panke, S. & Heinemann, M. Putative regulatory sites unraveled by network-embedded thermodynamic analysis of metabolome data. *Mol. Syst. Biol.* **2**, 2006.0034 (2006).
28. Jamshidi, N. & Palsson, B.A. Top-down analysis of temporal hierarchy in biochemical reaction networks. *PLOS Comput. Biol.* **4**, e1000177 (2008).
29. Chassagnole, C., Noisommit-Rizzi, N., Schmid, J.W., Mauch, K. & Reuss, M. Dynamic modeling of the central carbon metabolism of *Escherichia coli*. *Biotechnol. Bioeng.* **79**, 53–73 (2002).
30. Teusink, B., Walsh, M.C., van Dam, K. & Westerhoff, H.V. The danger of metabolic pathways with turbo design. *Trends Biochem. Sci.* **23**, 162–169 (1998).
31. Emmerling, M., Bailey, J.E. & Sauer, U. Altered regulation of pyruvate kinase or co-overexpression of phosphofructokinase increases glycolytic fluxes in resting *Escherichia coli*. *Biotechnol. Bioeng.* **67**, 623–627 (2000).
32. Meyer, D., Schneider-Fresenius, C., Horlacher, R., Peist, R. & Boos, W. Molecular characterization of glucokinase from *Escherichia coli* K-12. *J. Bacteriol.* **179**, 1298–1306 (1997).

33. Cho, B.-K. *et al.* The transcription unit architecture of the *Escherichia coli* genome. *Nat. Biotechnol.* **27**, 1043–1049 (2009).
34. Güell, M. *et al.* Transcriptome complexity in a genome-reduced bacterium. *Science* **326**, 1268–1271 (2009).
35. Sharma, C.M. *et al.* The primary transcriptome of the major human pathogen *Helicobacter pylori*. *Nature* **464**, 250–255 (2010).
36. Holtz, W.J. & Keasling, J.D. Engineering static and dynamic control of synthetic pathways. *Cell* **140**, 19–23 (2010).
37. Gibson, D.G. *et al.* Enzymatic assembly of DNA molecules up to several hundred kilobases. *Nat. Methods* **6**, 343–345 (2009).
38. Fell, D. *Understanding the Control of Metabolism* (Portland Press, London, UK, 1997).
39. Stephanopoulos, G., Aristidou, A.A. & Nielsen, J. *Metabolic Engineering–Principles and Methodologies* (Academic Press, London, UK, 1998).
40. Delgado, J. & Liao, J.C. Determination of flux control coefficients from transient metabolite concentrations. *Biochem. J.* **282**, 919–927 (1992).
41. Delgado, J. & Liao, J.C. Metabolic control analysis using transient metabolite concentrations. Determination of metabolite concentration control coefficients. *Biochem. J.* **285**, 965–972 (1992).

Acknowledgments

We would like to thank N. Zamboni, U. Sauer, M. Oldiges and C. Wandrey for help with MS analyses. This work was supported by the EU-FP6 projects EUROBIOSYN and NANOMOT.

Author contributions

M.B. did the experiments and analyzed the data and wrote the manuscript with S.P., who also supervised the work. R.P. and M.S. helped to construct the setup, and M.H. supervised part of the work.

Competing financial interests

The authors declare no competing financial interests.

Additional information

Supplementary information is available online at http://www.nature.com/naturechemicalbiology/. Reprints and permissions information is available online at http://npg.nature.com/reprintsandpermissions/. Correspondence and requests for materials should be addressed to S.P.